한국지반공학회논문집 제17권 5호 2001년 10월 pp. 71 ~ 82

Anisotropic Modelling of Partially Saturated Soil Behaviour by Means of ALTERNAT

ALTERNAT 구성모델을 이용한 불포화토 거동의 비등방 모형화

Kwon, Hee-Cheol[*1] 권 희 철
Lee, Cheo-Keun[*2] 이 처 근
Heo, Yol[*3] 허 열

요 지

불포화토에 있어서 함수상태는 지반이 건조할수록 수축하고 습윤상태로 진행할수록 파괴에 이르게 하는 추가적인 입자간 응력을 발생시키며, 이러한 간극수와 흙입자 사이에 발생하는 현상을 규명하기 위해서는 정확한 모형화가 필요하다. 흙입자와 간극수 사이의 상호작용에서 흡입유발 유효응력(suction-induced effective stress)을 규명하기 위해 정규모형(regular packing)과 임의모형(random packing)이 적용될 수 있다. 최근의 연구결과에 따르면 흙은 흡입유발 유효응력과 밀접한 관계가 있으며, 흙의 비등방텐서(anisotropic tensor)를 구하기 위해 적용된 ALTERNAT 모델을 이용하여 구조텐서(fabric tensor)를 개략적으로 정의할 수 있다. Thornton의 임의모형 시뮬레이션은 구조텐서에 상응하는 파괴응력 상태를 포함하고 있으며, 미소역학 시뮬레이션을 통하여 구조텐서를 구하였다. 본 연구에서는 상기에 언급된 구형의 흙입자 모형에 대한 이론적 고찰이 수행되었고, ALTERNAT 모델을 적용한 간단한 비등방텐서의 결과를 구조텐서와 비교하였다. 본 연구결과 비등방텐서는 미소역학 시뮬레이션에 의한 구조텐서에 비해 약 20~40% 정도 큰 값을 나타내었다.

Abstract

In partially saturated soil the moisture induces additional intergranular stresses which cause loose soils to shrink when dried and to collapse when wetted. To take account of these phenomena the interaction between the pore water and the soil particles needs to be modelled properly. The interaction between soil particles and pore water can be applied to a regular packing and random packings to consider the suction-induced effective stress. Based on recent research it is understood that the soil fabric affects the suction-induced effective stress. In the ALTERNAT model an anisotropic tensor may be defined which approximates the fabric tensor. Thornton's simulations of random packing include the failure stress state and the corresponding fabric tensor in the micromechanical simulation. In this study the formulation of the suction-induced effective stress for both a regular packing and random packings of spheres are discussed. It enables a comparison between the fabric tensor in the micromechanical simulation and a proposed simple anisotropic tensor approximating the fabric tensor in ALTERNAT. The proposed simple anisotropic tensor is found to be 20~40% larger than the fabric tensor according to the micromechanical simulations.

Keywords : ALTERNAT, Anisotropic tensor, Fabric tensor, Partially saturatecd soil, Suction-induced effective stress

*1 Dept. of Civil Engrg., The Univ. of Manchester
*2 Member, Reseacher, Institute of Construction Technology, Chungbuk Univ.
*3 Member, Professor, Dept. of Civil Engrg., Chungbuk Univ.

1. Introduction

Partially saturated soil occurs in practice between the ground surface and roughly the groundwater table. To take advantage of effective stress-strain models as used for dry and fully saturated soil an effective stress concept for partial saturation would be paramount. To investigate the possibilities for such concept a micromechanical study is done to describe the interaction between the soil skeleton and the pore liquid as pore water and air with water vapour. This interaction must be expressed in continuum terms by means of an effective stress induced by pore suction. Such a continuum mechanical concept is needed to understand the effect of the pore suction on the stress-strain behaviour of the soil skeleton.

The aim of this paper is to formulate such suction-induced effective stress using the measured pore water suction together with a macroscopic measure of the anisotropic fabric of granular soils. For the fabric tensor in granular soils the formulation of the suction-induced effective stress of a regular packing and random packings of spheres are considered. To this end the ALTERNAT model will be applied to estimate an anisotropic tensor as a simple formulation. The results of the anisotropic tensor in the ALTERNAT model will be compared to the fabric tensor as simulated by Thornton (2000) for random packings of spheres. In this paper it is investigated whether these tensor can be used to formulate a continuum mechanical model for the suction-induced effective stress.

2. Interactions of Water Bridge and Water Vapour

2.1 Equilibrium of the Gas-liquid Interface

The pressure difference for a warped gas-liquid interface, as a function of surface tension and curvature, has been derived by Laplace(1806) (Nazemi, 1998). If $R_1 \neq R_2$ the mean radius of the interface curvature R' can be expressed by:

$$\frac{2}{R'} = \frac{1}{R_1} + \frac{1}{R_2} \tag{1}$$

thus the Laplace equation becomes:

$$\psi = \frac{2\sigma}{R'} \tag{2}$$

Laplace equation may be changed due to the existence of surface tension, σ. An arbitrary surface of mean radius of curvature R' depends on mechanical equilibrium between two fluids at different pressures p_g and p_w. A plane surface, therefore, can exist only when the pressures of the fluid on the two different sides are equal. If the two centres of curvature are on both sides of the saddle-shaped surface as illustrated in Fig. 1, the pressure difference ψ is expressed by:

$$\psi = \sigma\left(\frac{1}{R_1} - \frac{1}{R_2}\right) \tag{3}$$

The intersection of the gas-liquid interface with a plane through the centroid of the spheres is a plane curve y = f(x). The radius of curvature r for a point P on a plane curve is given by (Molenkamp & Nazemi, 2000):

$$r = \left| \frac{\left[1 + \left(\frac{dy}{dx}\right)^2\right]^{3/2}}{\frac{d^2y}{dx^2}} \right| \quad \left(\frac{d^2y}{dx^2} \neq 0\right) \tag{4}$$

To describe the shape of the liquid bridge as illustrated in Fig. 2 and the corresponding pressure deficiency across the gas-liquid interface in equation (3) for $R_1 = r$ according to equation (4) is substituted while the radius R_2 can be expressed by:

$$R_2 = y\left[1 + \left(\frac{d^2y}{dx^2}\right)^2\right]^{1/2} \tag{5}$$

After substitution of equation (4) and (5) in equation (3) the capillary suction ψ can be written as follows (Hotta, Takeda & Iiniya, 1974)

$$\frac{\psi}{\sigma} = \frac{\frac{d^2y}{dx^2}}{\left[1 + \left(\frac{dy}{dx}\right)^2\right]^{3/2}} - \frac{1}{y\left[1 + \left(\frac{dy}{dx}\right)^2\right]^{1/2}} \tag{6}$$

From the shape of the liquid bridge as illustrated in Fig. 2 the dimensionless capillary suction Ψ can be written as follows

$$\Psi = \frac{\psi R}{\sigma} = \frac{\frac{d^2Y}{dX^2}}{[1+(\frac{dY}{dX})^2]^{3/2}} - \frac{1}{Y[1+(\frac{dY}{dX})^2]^{1/2}} \tag{7}$$

where $X(=x/R)$ and $Y(=y/R)$ are dimensionless coordinates with respect to the sphere radius R. The dimensionless capillary suction Ψ shows the effect of the difference in the gas pressure and the liquid pressure. If the liquid pressure is larger than the gas pressure, the sign is negative.

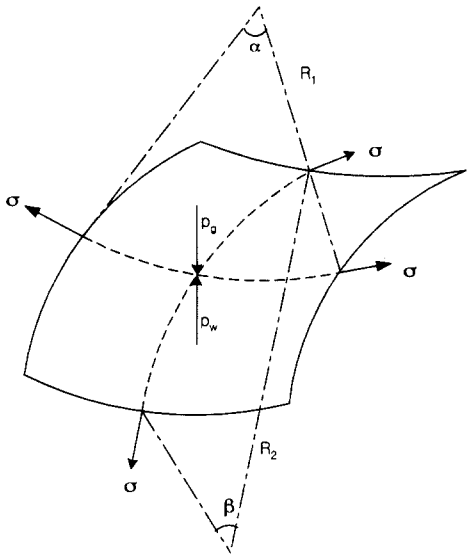

Fig. 1. Surface tension on a curved interface with centre on different side

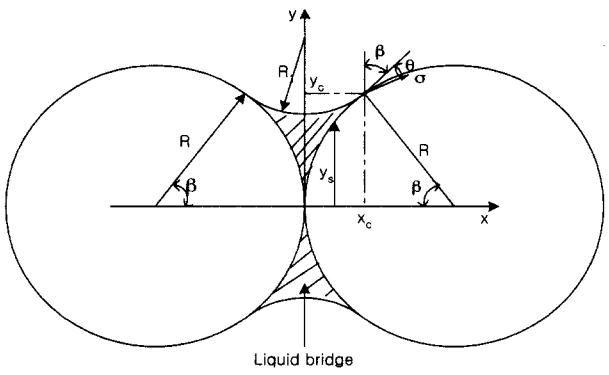

Fig. 2. A symmetric liquid bridge between two equal rigid spheres

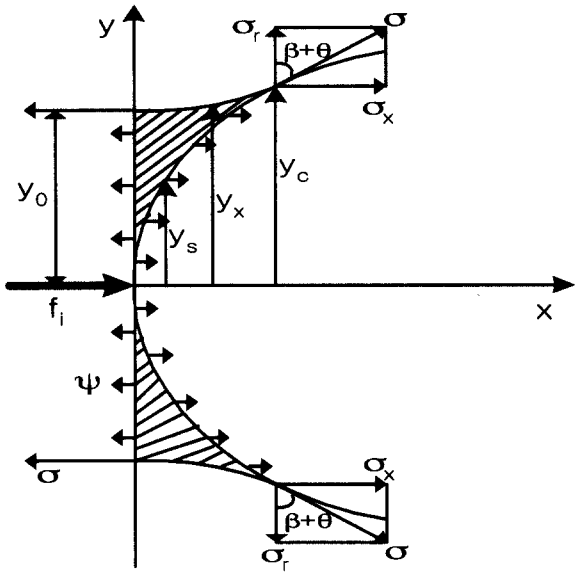

Fig. 3. Section of a symmetric liquid bridge in contact with a rigid sphere

2.2 Equilibrium of the Spheres and the Liquid Bridge

Fig. 3 describes the geometry of the right hand side half of liquid bridge with neck radius y_0, the y-coordinate of the point y_x on the gas-liquid interface at ordinate x, the radius y_s of the interface with the right sphere at x. Both surfaces intersect at x-coordinate x_c and y-coordinate y_c. The capillary suction ϕ and the direct interparticle force f between the spheres can be calculated depending on the amount of water in between the spheres.

In the absence if gravitational effects of equilibrium of the liquid profile and buoyancy effect involves three conditions. This condition involves the total load through the mid-plane between the spheres as illustrated by means of Fig. 3. The total force in x-direction through the mid-plane between the spheres must be zero because the right side sphere in Fig. 2 does not accelerate. In this case the dimensionless capillary suction Ψ can be described as a function of the liquid-solid contact angle θ and the dimensionless neck and contact radii Y_0 and Y_c, namely (Nazemi & Molenkamp, 1999)

$$\Psi = \frac{2Y_0 - 2Y_c(Y_c\cos\theta + \sin\theta\sqrt{1-Y_c^2}}{Y_c^2 - Y_0^2} \tag{8}$$

3. Partially Saturated Pyramidal Packings of Spheres

3.1 REV of Pyramidal Packing

A physical model may be used to consider the micromechanical relation between the saturation, the pore suction and the soil induced intergranular, or effective stress in a granular skeleton. The model is considered as a regular pyramidal packing of isodiametrical spheres with radii R. These idealized soils consist of layers on a square grid with a grid size 2Rb, in which b (≥ 1) is the width parameter. In subsequent horizontal layers the grid is moved by half a grid size in both directions so that a sphere of a subsequent layer falls in the hollow between the four sphere of the layer underneath (Molenkamp & Nazemi, 2000). A Representative Elementary Volume (REV) of pyramidal packing is described in Fig. 4 and Fig. 5.

3.2 Suction-Induced Effective Stress in Pyramidal Packing

At a low saturation the effective stresses due to the water bridges in the regular packing involve only the normal suction forces. The normal forces N is on the eight diagonal contact points of each sphere are indicated by f. When $h = 1$ the vertical normal forces N^v is equal to the vertical contact forces f^v on the two vertical contact points of each sphere. When $h = \sqrt{2}$ the normal horizontal forces N^h are equal to the horizontal contact forces f^h on the four horizontal contact points per sphere.

The suction induced interparticle force f between two spheres can be expressed in dimensionless form by quantity F, namely (Molenkamp & Nazemi, 2000):

$$F = \frac{f}{\sigma R} = \text{function}(\Psi, \theta, S) \tag{9}$$

where Ψ is the dimensionless capillary suction, θ is the liquid-solid surface contact angle and S is the dimensionless sphere half-separation. The effective pore suction ϕ' can be expressed in dimensionless terms as well. The expressions are (Molenkamp & Nazemi, 2000)

$$\Psi'_{11} = \frac{\phi'_{11} R}{\sigma} = \frac{F h}{4 - h^2} \left[+ \frac{F^v}{3} \text{ if } h = 1 \right] \tag{10}$$

and

$$\Psi'_{22} = \Psi'_{33} = \frac{F}{2h} \left[+ \frac{F^h}{2\sqrt{2}} \text{ if } h = \sqrt{2} \right] \tag{11}$$

3.3 Fabric Tensor, Neutral Stress State and Failure State in Pyramidal Packing

The geometry of the pyramidal packing as illustrated in Fig. 5 shows that the diagonals COE and DOF are always constant, namely $4R$ because the spheres if the

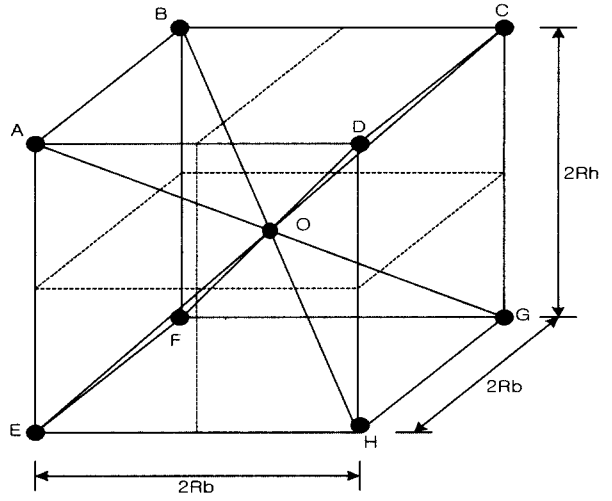

Fig. 4. Geometry of REV of pyramidal packing of spheres with radius R

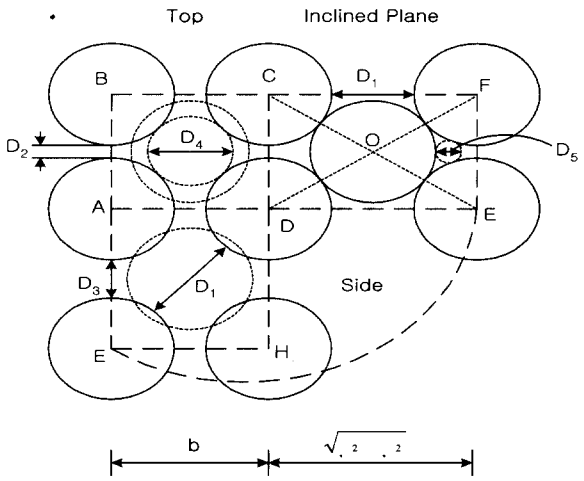

Fig. 5. Scaled geometry of the pyramidal packing

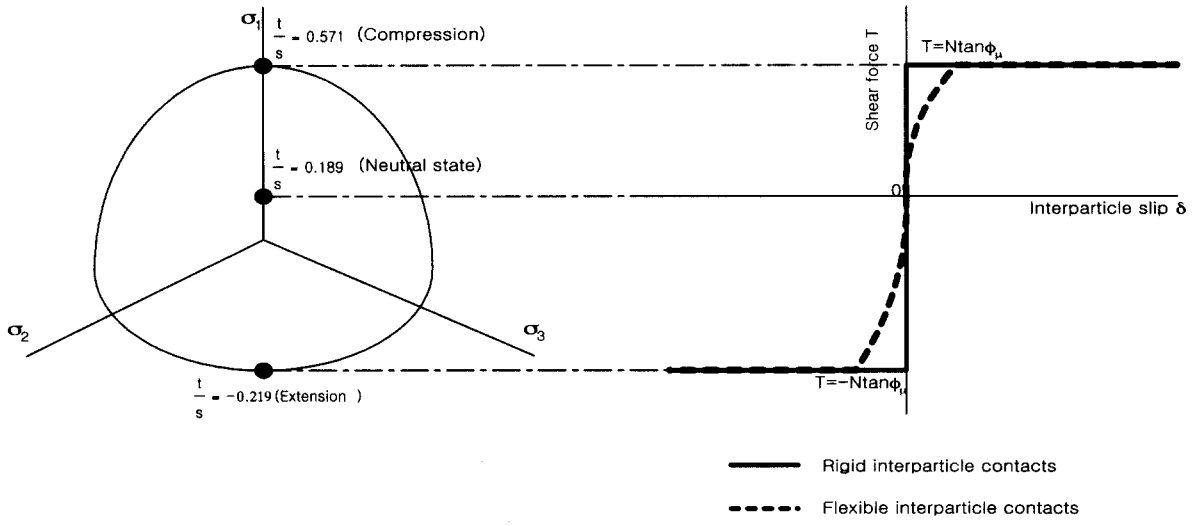

(a) In terms of shear stress level(t/s) (b) In terms of interparticle force

Fig. 6. Neutral and failure stress state for triaxial compression and extension for pyramidal packing with parameter h=1.3

pyramidal packing are considered to be rigid. Consequently the width parameter b will increase and the height parameter h will decrease during triaxial compression.

If $h = 1.3$ the mobilized friction angle can be calculated by (Molenkamp & Nazemi, 2000):

$$\sin\phi = \frac{3h^2 - 4}{h^2 + 4} \tag{12}$$

The shear stress level can be calculated by:

$$\frac{t}{s} = \frac{2\sqrt{2}\sin\phi}{3 - \sin\phi} \tag{13}$$

Thus, for $h = 1.3$ the mobilized friction angle $\phi = 10.84$ if the shear stress $T = 0$. This indicates the mobilized friction angle at the neutral stress state . This clarifies that the stress due to normal contact forces N not only has an isotropic part but it can also have a deviatoric part, depending on the fabric tensor.

During vertical compression the interparticle shear forces T are $T = N\tan\phi_\mu$ and during vertical extension they are $T = -N\tan\phi_\mu$. If the maximum interparticle friction angle $\phi_\mu = 20^\circ$ and $h = 1.3$ the mobilized friction angle and the shear stress level, t/s, are calculated as shown Table 1.

Table 1. The value of three parameters

Obtained value	Neutral	Compression	Extension
sin ϕ	0.188	0.504	−0.219
Friction angle(°)	10.84	30.25	−12.65
t/s	0.189	0.571	−0.192

Fig. 6 shows these stress levels together with yield surface in the π-plane. In addition the relationship between the interparticle shear forces and the interparticle slip movement is indicated in general terms. The neutral stress state is indicated in the π-plane as well.

4. Partially Saturated Random Packings of Spheres

In random packings the number of contact points C. The volume of the REV varies per particle selected sufficiently large, e.g. containing 1000 particles. The intergranular stress tensor in random packings for the pyramidal packing is written as (Thornton, 2000):

$$\sigma_{ij}^{R'} = \frac{2}{V} N^R R \sum_1^C n_i n_j + \frac{2}{V} T^R R \sum_1^C t_i n_j \tag{14}$$

where N^R and T^R are the normal and tangential contact force in random packing, respectively. The superscript R indicates the random packing, V is the volume of REV and R is the radius of sphere, which is the same for all spheres. N^R, T^R and R are constant.

Equation (14) can be expressed as follows:

$$\sigma_{ij}^{R\prime} = \frac{2N^R R}{V}\nu_{ij} + \frac{2T^R R}{V}\tau_{ij} \tag{15}$$

where

$$\nu_{ij} = \sum_{1}^{c} n_i n_j \tag{16}$$

$$\tau_{ij} = \sum_{1}^{c} t_i n_j \tag{17}$$

When expressed with respect to principal stress axis the principal effective stress components can be obtained according to equation (15) as:

$$\sigma_{11}^{R\prime} = \frac{2N^R R}{V}\nu_{11} + \frac{2T^R R}{V}\tau_{11} \tag{18}$$

$$\sigma_{22}^{R\prime} = \frac{2N^R R}{V}\nu_{22} + \frac{2T^R R}{V}\tau_{22} \tag{19}$$

$$\sigma_{33}^{R\prime} = \frac{2N^R R}{V}\nu_{33} + \frac{2T^R R}{V}\tau_{33} \tag{20}$$

while the shear stresses are zero. For triaxial stress state $\sigma_{22}^{R\prime} = \sigma_{33}^{R\prime}$, as also considered for the regular pyramidal packing.

In random packings for low saturation and without the application of any external load the interparticle forces due to the individual water bridges includes only the suction-induced normal force, namely $N^R = f^R$, as mentioned before for the regular pyramidal packing. The suction-induced intergranular stress tensor according to equations (18), (19) and (20) reads:

$$\psi_{11}^{R\prime} = \frac{2Rf^R}{V}\nu_{11} \tag{21}$$

$$\psi_{22}^{R\prime} = \frac{2Rf^R}{V}\nu_{22} \tag{22}$$

$$\psi_{33}^{R\prime} = \frac{2Rf^R}{V}\nu_{33} \tag{23}$$

Each suction-induced effective stress $\psi_{ij}^{R\prime}$ component is depends on the fabric tensor component ν_{ij}.

5. Anisotropy of Granular Packing and Kinematic Rule in ALTERNAT

The effective stress σ_{ij} in a granular material is due to both the interparticle normal forces N and the interparticle shear forces T. However, in contrast to the case of a regular packing of spheres in a granular material both types of forces will always occur simultaneously as a consequence of the equilibrium conditions of all individual irregularly shaped particles arranged in an irregular granular skeleton.

Nevertheless, the magnitude of the interparticle shear forces T increase as the stress state approaches failure. In such case at an increasing number of contacts the failure criterion of interparticle slip must be reached, namely:

$$T = N\tan\phi_\mu \tag{24}$$

in which ϕ_μ is the interparticle friction angle.

Next consider the stress state for which the shear forces T are minimum. In such case any very small deformation will almost be elastic, because hardly any of the interparticle forces will reach the local slip limit and so hardly any interparticle contact will slip. This state is indicated as the neutral state.

A so-called neutral stress state is indicated by:

$$\sigma_{ij}^{n} = p(\delta_{ij} + \xi_{ij}) \tag{25}$$

in which p is the mean effective stress, δ_{ij} are the second order isotropic tensor components and ξ_{ij} are the second order deviatoric tensor components describing the deviatoric stress components at the neutral state in a dimensionless form. Consequently $\xi_{ij}\delta_{ij} = 0$.

The deviatoric stress with respect to the neutral stress state is indicated by the additional deviatoric stress X_{ij} which is due to the change of the interparticle shear forces T towards slip. Consequently any non-neutral effective stress state can be expressed as:

$$\sigma_{ij} = X_{ij} + p(\delta_{ij} + \xi_{ij}) \tag{26}$$

In the ALTERNAT model (Molenkamp, 1982) this decom- position is expressed as follows:

$$\sigma_{ij} = T_{ij} + p\xi_{ij} \tag{27}$$

in which $p\xi_{ij}$ is deviatoric stress representing the anisotropy of the soil skeleton and,

$$T_{ij} = X_{ij} + p\delta_{ij} \tag{28}$$

which represents the stress components inducing shearing and volume change and is called the pseudo stress.

The neutral stress state σ^n specifies the centre of the yield surface in the π-plane. The deviatoric component X_{ij} of the pseudo-stress T_{ij} specifies the magnitude of the yield surface in the π-plane.

At any stress state on the yield surface the plastic stiffness is specified. The distribution of the plastic stiffness within the maximum surface is specified through the various anisotropy tensors and stress reversal points, which together define a kinematic yield surface through any stress point. In general the plastic stiffness decreases with increasing size of the yield surface.

Lade and Duncan (1975) give an expression of a yield surface F, namely:

$$F = \frac{I_1^3}{I_3} - 27 - f(\chi) = 0 \tag{29}$$

where $f(\chi)$ is the size of the yield surface, χ is the kinematic hardening parameter and I_1 and I_3 are the first and third invariants of the stress.

Fig. 7 shows a typical stress-strain response for cyclic loading involving consecutive branches of triaxial extension and compression. The shapes and locations of the yield surfaces corresponding to every state indicated in Fig. 7 are illustrated in Fig. 8.

Starting at the initial neutral K0 stress point A, the smallest yield surface increases in a pseudo isotropic way as shown in Fig. 8(a) and Fig. 8(b). The deviatoric stress decreases from point A along point B until reaching the isotropic point C in Fig. 8(c). During reloading in triaxial compression to point D the deviatoric stress is increased

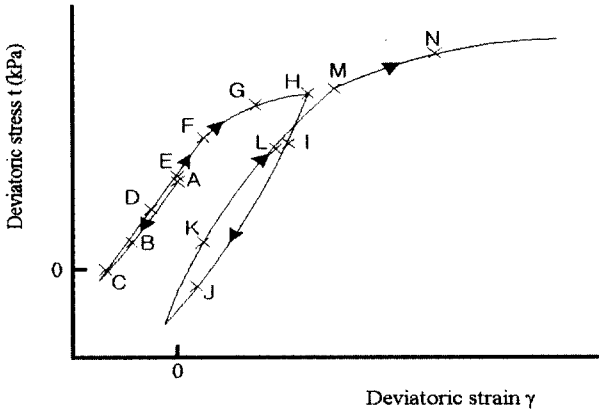

Fig. 7. Typical relationship between deviatoric strain and deviatoric stress for cyclic loading

and a new small yield surface is created from the isotropy point onwards as shown in Fig. 8(d). When the active yield surface reaches the next encompassing yield surface the latter is erased. When the deviatoric stress increases further until point H then all yield surfaces are erased except the largest isotropic yield surface as indicated in Fig. 8(h).

When the material would be loaded monotonically towards *failure* the kinematic yield surface would expand towards the peak shear stress level and would shrink subsequently to reach eventually the critical state.

Unloading from point H to a negative deviatoric stress follows as e.g. point J in Fig. 7 causes the two yield surfaces as shown Fig. 8(j). Points K, L, M and N are located on a similar reloading stress-strain path as the stress points D to H. During the unloading and reloading sequence, expansion, erasure and generation of the different yield surfaces can be observed.

6. Suction Induced Anisotropy Tensor in ALTERNAT

The suction-induced effective stress $\phi_{ij}^{R'}$ has an isotropic and deviatoric part as described by equations (21), (22) and (23), namely

$$\phi_p^{R'} = \frac{\phi_{11}^{R'} + \phi_{22}^{R'} + \phi_{33}^{R'}}{3} = \frac{2Rf^R}{3V}(\nu_{11} + \nu_{22} + \nu_{33}) \tag{30}$$

$$\phi_q^{R'} = \phi_{11}^{R'} - \phi_{33}^{R'} = \frac{2Rf^R}{V}(\nu_{11} - \nu_{33}) \tag{31}$$

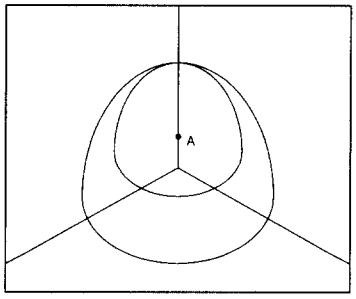

(a) At point A: initial state

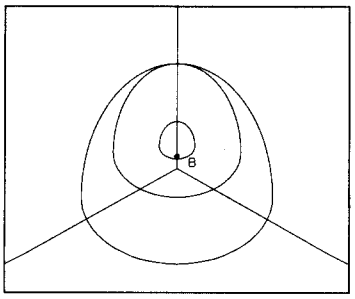

(b) At point B: Unloading

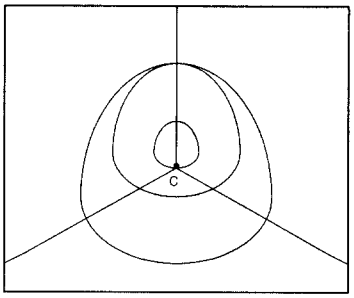

(c) At point C: Unloading
(Zero of deviatoric stress)

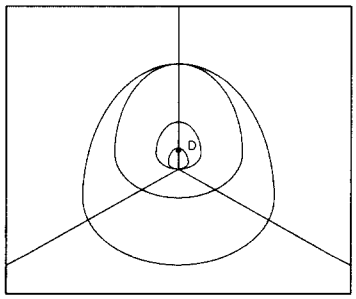

(d) At point D: Reloading

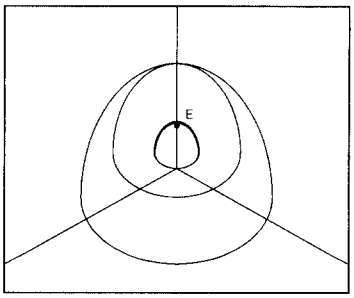

(e) At point E: Reloading

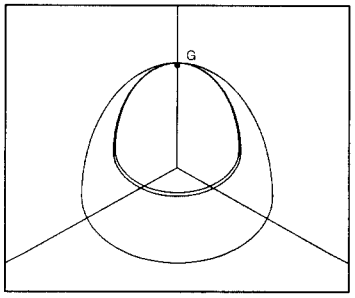

(f) At point F: Loading

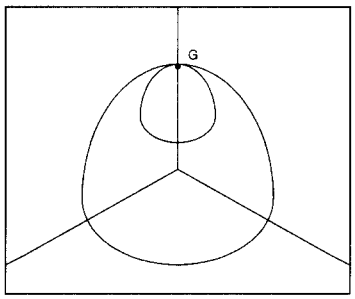

(g) At point G:Loading

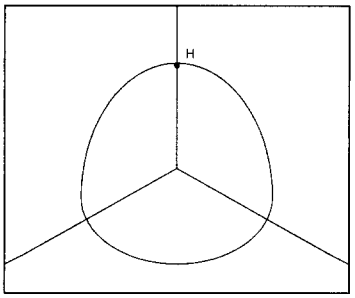

(h) At point H:Loading

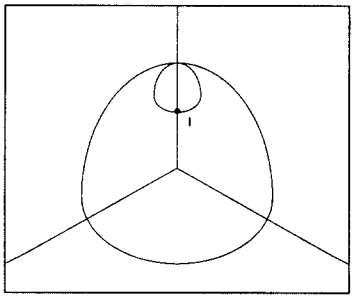

(i) At point I:Unloading

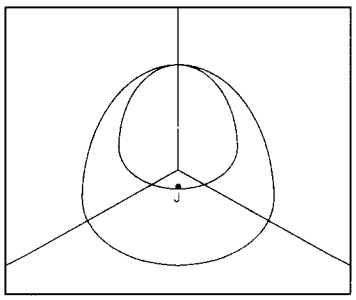

(j) At point J: Unloading

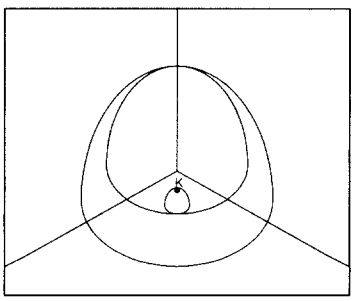

(k) At point K: Reloading

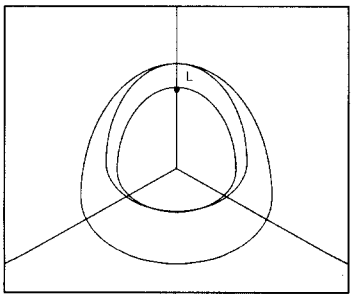

(l) At point L: Reloading

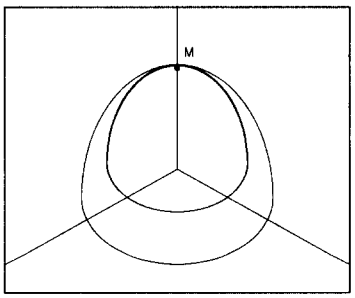

(m) At point M: Loading

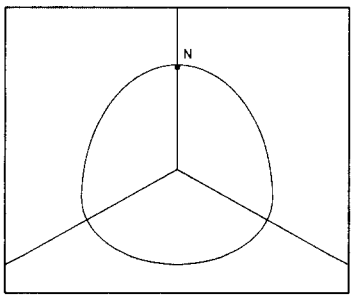

(n) At point N: Loading

Fig. 8. Typical yield surface movement for cyclic loading and triaxial stress states(Dots indicate current active stress location)

If the fabric tensor with components ν_{ij} can be estimated and the mean suction-induced effective stress $\phi_p^{R'}$ can be measured, then from the above equations the corresponding deviatoric part of the suction-induced stress can be calculated, namely:

$$\phi_q^{R'} = 3\left[\frac{\nu_{11} - \nu_{33}}{\nu_{11} + \nu_{22} + \nu_{33}}\right]\phi_p^{R'} \tag{32}$$

in which the interparticle suction-induced force f^R, the radius of the particles R and the volume V of REV do not occur.

In order to enable the application of this calculation the fabric tensor needs to be estimated. Next the suitability of a simple procedure to estimate the fabric tensor using the ALTERNAT model is evaluated. To this end Thornton's (2000) results of failure are used as a basis for comparison to establish the quality of the proposed simple ALTERNAT procedure.

The failure surface of Thornton's (2000) simulation in Fig. 9 is centred with respect to the isotropic point D in the π -plane. During initial loading in triaxial compression the fabric tensor increases from the isotropic state represented by point D to the anisotropic state represented by point C in Fig. 9 for a stress state corresponding to peak point A. Thus for this peak stress A the corresponding fabric tensor is represented by point C.

The purpose of the following consideration is to find a method to estimate the anisotropic tensor for the failure stress state. Thornton above mentioned results can be used to evaluate the suitability of such method. The envisaged method is based on the ALTERNAT model formulation. In fact it is proposed to consider the anisotropic tensor obtained by subsequent unloading from peak stress point A to the isotropic stress state represented by point D in Fig. 9(a). In this figure the resulting yield surface is indicated together with its anisotropic tensor as represented by point B. The aim of the exercise is to determine the difference between the anisotropic tensor indicated by point B and the fabric tensor represented by point C.

As point C has been calculated by Thornton (2000) for the random packing of spheres any deviation of point B with respect to point C will mean a short coming of the proposed concept for the ALTERNAT model.

Fig. 9(a) shows the current active yield surface between the peak failure point A and isotropic point D for unloading after triaxial compression. For unloading after triaxial extension in the Fig. 9(b) the active yield surface reaches from the bottom failure point G to the isotropic point D.

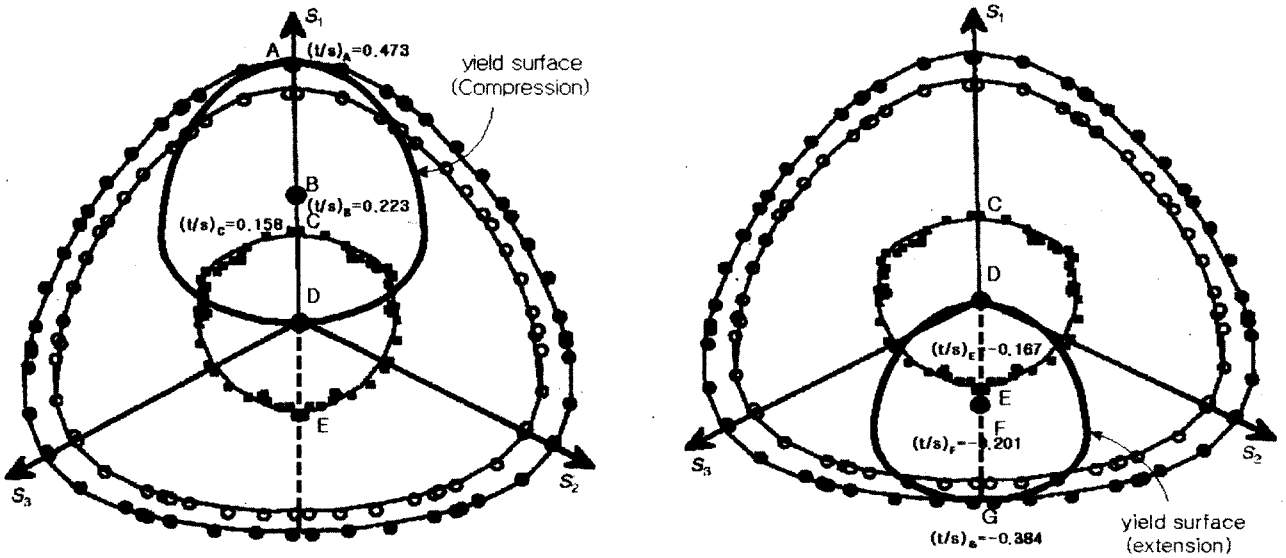

(a) For triaxial compression (b) For triaxial extension

Fig. 9. The relation between fabric tensor and anisotropic tensor in terms of yield surfaces(Failure state of stress-●, normal contact force contribution-○ and fabric stress component-■)

The axial and radial stresses for triaxial stress states have been expressed in terms of isotropic stress s and shear stress level t/s (Woodward & Molenkamp, 1999), namely:

$$\sigma_r = s\left(\frac{1}{\sqrt{3}} - \frac{1}{\sqrt{6}}\frac{t}{s}\right) \quad (33)$$

$$\sigma_a = s\left(\frac{1}{\sqrt{3}} + \sqrt{\frac{2}{3}}\frac{t}{s}\right) \quad (34)$$

The size of the Lade and Duncan (1975) yield surface is expressed in terms of parameter η, namely:

$$\eta = \frac{I_1^3}{I_3} - 27 \quad (35)$$

where for triaxial compression the first stress invariant is:

$$I_1 = \sigma_a + 2\sigma_r \quad (36)$$

and the third stress invariant is:

$$I_3 = \sigma_a \sigma_r^2 \quad (37)$$

Substituting the equations (33) and (34) into equations (36) and (37), respectively, I_1 and I_3 are as follows:

$$I_1 = \frac{s}{\sqrt{3}} + \sqrt{\frac{2}{3}}t + \frac{2s}{\sqrt{3}} - \frac{2}{\sqrt{6}}t = s\sqrt{3} \quad (38)$$

$$I_3 = \left(\frac{s}{\sqrt{3}} + \sqrt{\frac{2}{3}}t\right)\left(\frac{s}{\sqrt{3}} - \frac{t}{\sqrt{6}}\right)^2 \quad (39)$$

In Thornton's (2000) numerical simulations of the behaviour of random packing of spheres the size of the failure surface for dense packings $\eta = 9.53$. The deviatoric stress level (t/s) corresponding to $\eta = 9.53$ can be calculated by substituting equations (38) and (39) into equation (35). The result is as follows:

$$\eta = \frac{\sqrt{3}^3}{\left(\frac{1}{\sqrt{3}} + \sqrt{\frac{2}{3}}\frac{t}{s}\right)\left(\frac{1}{\sqrt{3}} - \sqrt{\frac{1}{6}}\frac{t}{s}\right)^2} - 27 = 9.53 \quad (40)$$

The deviatoric stress levels (t/s) at the peak failure surface for both triaxial compression and extension were calculated as:

$$\left(\frac{t}{s}\right)_{comp} = 0.473 \quad (41)$$

and

$$\left(\frac{t}{s}\right)_{ext} = -0.384 \quad (42)$$

This enables to find the applied scale in Fig. 9.

The deviatoric stress levels (t/s) at the centres of the anisotropy yield surfaces, obtained from unloading from peak states to the isotropic stress state, are indicated as point B and F in Fig. 9. In order to calculate the anisotropy of point B it should be recognised that in Fig. 9 the size η_{comp} of the yield surface through points A and D is the same.

In the ALTERNAT model to find the anisotropy the stress state should be represented as expressed by equation (27). According to equation (27) the axial and the radial stresses read:

$$\sigma_a = T_a + p\xi_a \quad (43)$$

$$\sigma_r = T_r + p\xi_r \quad (44)$$

where T_{ij} is the pseudo stress as defined in equation (28), p is the mean stress and ξ_{ij} is an anisotopic tensor. The term $p\xi_{ij}$ is the deviatoric stress representing the anisotropy of the soil skeleton. Thus,

$$T_a = \sigma_a - p\xi_a \quad (45)$$

$$T_r = \sigma_r - p\xi_r \quad (46)$$

The size η_{comp} of yield surface for unloading from compression as shown Fig. 9(a) can be determined from:

$$\eta_{comp} = \frac{(T_a + 2T_r)^3}{T_a T_r^2} - 27 \quad (47)$$

in which T_a and T_r are the pseudo stresses, which are to be considered for both points A and D.

Substituting equations (45) and (46) into the equation (47) leads to:

$$\eta_{comp} = \frac{\left[\left(\sigma_a - \frac{1}{\sqrt{3}}\xi_a\right) + 2\left(\sigma_r - \frac{1}{\sqrt{3}}\xi_r\right)\right]^3}{\left(\sigma_a - \frac{1}{\sqrt{3}}\xi_a\right)\left(\sigma_r - \frac{1}{\sqrt{3}}\xi_r\right)^2} - 27 \quad (48)$$

where

$$\xi_a + 2\xi_r = 0 \tag{49}$$

due to the anisotropy being a deviatoric tensor.

Substituting equations (33), (34) and (49) into equation (48) leads to:

$$\eta_{comp} = \frac{\left[\left(\frac{1}{\sqrt{3}} + \sqrt{\frac{2}{3}}\frac{t}{s} - \frac{1}{\sqrt{3}}\xi_a\right) + 2\left(\frac{1}{\sqrt{3}} - \frac{1}{\sqrt{6}}\frac{t}{s} + \frac{1}{2\sqrt{3}}\xi_a\right)\right]^3}{\left(\frac{1}{\sqrt{3}} + \sqrt{\frac{2}{3}}\frac{t}{s} - \frac{1}{\sqrt{3}}\xi_a\right)\left(\frac{1}{\sqrt{3}} + \frac{1}{\sqrt{6}}\frac{t}{s} - \frac{1}{2\sqrt{3}}\xi_a\right)^2} - 27 \tag{50}$$

Since the value of η_{comp} is the same for both points A and D from the equation (50) the following expression is obtained:

$$\frac{\left[\left(\frac{1}{\sqrt{3}} + \sqrt{\frac{2}{3}}\left(\frac{t}{s}\right)_A - \frac{1}{\sqrt{3}}\xi_a\right) + 2\left(\frac{1}{\sqrt{3}} - \frac{1}{\sqrt{6}}\left(\frac{t}{s}\right)_A + \frac{1}{2\sqrt{3}}\xi_a\right)\right]^3}{\left(\frac{1}{\sqrt{3}} + \sqrt{\frac{2}{3}}\left(\frac{t}{s}\right)_A - \frac{1}{\sqrt{3}}\xi_a\right)\left(\frac{1}{\sqrt{3}} + \frac{1}{\sqrt{6}}\left(\frac{t}{s}\right)_A - \frac{1}{2\sqrt{3}}\xi_a\right)^2} = \frac{\left[\left(\frac{1}{\sqrt{3}} + \sqrt{\frac{2}{3}}\left(\frac{t}{s}\right)_D - \frac{1}{\sqrt{3}}\xi_a\right) + 2\left(\frac{1}{\sqrt{3}} - \frac{1}{\sqrt{6}}\left(\frac{t}{s}\right)_D + \frac{1}{2\sqrt{3}}\xi_a\right)\right]^3}{\left(\frac{1}{\sqrt{3}} + \sqrt{\frac{2}{3}}\left(\frac{t}{s}\right)_D - \frac{1}{\sqrt{3}}\xi_a\right)\left(\frac{1}{\sqrt{3}} + \frac{1}{\sqrt{6}}\left(\frac{t}{s}\right)_D - \frac{1}{2\sqrt{3}}\xi_a\right)^2} \tag{51}$$

where $(t/s)_A = 0.473$ and $(t/s)_D = 0$.

Enabled the calculation of ξ_a^{comp}, namely:

$$\xi_a^{comp} = 0.316 \tag{52}$$

Subsequent application of equation (49) gives:

$$\xi_r^{comp} = -0.158 \tag{53}$$

The anisotropy of point D for the unloading from triaxial extension has been obtained in the same way, leading to:

$$\xi_a^{ext} = -0.284, \quad \xi_r^{ext} = 0.142 \tag{54}$$

Substituting the value of ξ_a^{comp} according to equations (52) and (53) into equation (50) gives for the size of yield surface $\eta_{comp} = 2.43$. Similarly, for ξ_a^{ext} according to equation (53) the size of yield surface $\eta_{ext} = 1.56$ is found.

Finally the deviatoric stress levels (t/s) of points B and F can be calculated. It is noted that for these points the deviatoric part of the pseudo stress X_{ij} in equation (28) is zero, thus $X_{ij} = 0$. Consequently (see equation (43) and (44)):

$$\sigma_a = p(\xi_a + 1), \quad \sigma_r = p(\xi_r + 1) \tag{55}$$

$$\sigma_a - \sigma_r = p(\xi_a - \xi_r) \tag{56}$$

where $p = s/\sqrt{3}$.

The deviatoric stress level (t/s) can expressed as (Woodward & Molenkamp, 1999):

$$\sqrt{\frac{3}{2}}\, t = \frac{s}{\sqrt{3}}\left(\xi_a^{comp} - \xi_r^{comp}\right) \tag{57}$$

thus,

$$\left(\frac{t}{s}\right)_B = \frac{1}{\sqrt{3}}\sqrt{\frac{2}{3}}\left(\xi_a^{comp} - \xi_r^{comp}\right) = \frac{1}{\sqrt{3}}\sqrt{\frac{2}{3}}(0.316 + 0.158) = 0.223 \tag{58}$$

Likewise, the triaxial extension case can be elaborated as:

$$\left(\frac{t}{s}\right)_F = \frac{1}{\sqrt{3}}\sqrt{\frac{2}{3}}\left(\xi_a^{ext} - \xi_r^{ext}\right) = \frac{1}{\sqrt{3}}\sqrt{\frac{2}{3}}(-0.284 - 0.142) = -0.201 \tag{59}$$

Since the deviatoric stress level (t/s) of points A, B, F, and G are calculated the deviatoric stress level (t/s) of points C and E may be estimated by considering the same scale in Fig. 9. For the triaxial compression the scaled estimation of point C can be calculated by results of $(t/s)_A$ and $(t/s)_B$, leading to approximately $(t/s)_C = 0.158$. Similarly, for the triaxial extension $(t/s)_E = -0.201$.

Consequently, the percentage of each shear stress level for triaxial compression reduces to:

$$\frac{(t/s)_B}{(t/s)_A} = \frac{0.223}{0.473} \times 100 = 47.1\%, \quad \frac{(t/s)_C}{(t/s)_A} = \frac{0.158}{0.473} \times 100 = 33.4\% \tag{60}$$

thus $(t/s)_B = 47.1\%$ and $(t/s)_C = 33.4\%$ of $(t/s)_A$.

For triaxial extension it reduces to:

$$\frac{(t/s)_E}{(t/s)_G} = \frac{-0.167}{-0.384} \times 100 = 43.5\%, \quad \frac{(t/s)_F}{(t/s)_G} = \frac{-0.201}{-0.384} \times 100 = 52.3\% \tag{61}$$

thus $(t/s)_E = 43.5\%$ and $(t/s)_F = 52.3\%$ of $(t/s)_G$.

The shear stress level of the anisotropic tensor of ALTERNAT as a function of the failure value is 13.7% larger for triaxial compression and 8.8% larger for triaxial extension.

This demonstrates that the proposed simple ALTERNAT concept of estimating the fabric tensor may not be accurate. The deviator part of the suction-induced effective stress as estimated by means of the proposed simple ALTERNAT concept would be a factor $(t/s)_B/(t/s)_C = 1.4$ larger for triaxial compression and a factor $(t/s)_F/(t/s)_E = 1.2$ larger for triaxial extension than the corresponding deviatoric part of the fabric tensor of the packings of spheres as calculated by Thornton (2000).

Consequently the proposed simple ALTERNAT procedure may over estimate the deviatoric part of the suction-induced effective stress by possibly 20~40%. The ideal result of the anisotropic tensor might be similar to the fabric tensor. However, the estimation of the deviatoric part of the suction-induced effective stress is different due to analytical methods between Thornton's simulation and the ALTERNAT modelling.

7. Conclusion

The behaviour of partially saturated soils is affected by the movement of vapour, water and heat. The deformation of loose soils includes phenomena as collapse due to wetting and shrinkage due to drying. The interaction between spheres, water bridge and water have been discussed starting from micromechanical considerations. In both regular and random packings the fabric tensor has been introduced and according to the micromechanical consideration a generalised effective stress concept has been formulated for partial saturation. It has been shown that the fabric tensor affects strongly the suction-induced effective stress in granular packings.

To describe these interactions in continuum mechanical terms the anisotropy as applied in the ALTERNAT model has been reviewed. The anisotropic tensor in ALTERNAT heavily depends on a kinematic rule designed to enable the definition of the plastic soil stiffness for any stress history and any stress rate. To arrive at a measure of the suction-induced effective stress tensor in the ALTERNAT model a simple formulation to estimate a fabric tensor in the ALTERNAT model has been proposed. The results according to this simple procedure, involving the definition of an anisotropic tensor, are compared to the fabric tensor as calculated by Thornton (2000) for random packings of spheres. For failure in triaxial compression and extension as considered, the method of defining a representative anisotropic tensor in ALTERNAT has been shown to give 20~40% larger shear stress levels due to suction than calculated by Thornton (2000) for random packings of spheres.

References

1. Hotta, K., Takeda, K. and Iinoa, K. (1974), "The Capillary Binding Force of a Liquid Bridge", Powder Technology, 10, pp.231~242.
2. Lade, P.V. and Duncan, J.M. (1975), "Elasto-plastic Stress-Strain Theory for Cohesionless Soils", J. Geotech. Engn. Div., ASCE, 107, pp.1037~1052.
3. Molenkamp, F. and Nazemi, A.H. (1999), Interactions between Two Spheres, Water Bridge and Water Vapour, UMIST, Research Report.
4. Molenkamp, F. and Nazemi, A.H. (2000), Micromechanical Considerations on Effective Stress Concept for Partially Saturated Granular Materials, UMIST, Research Report.
5. Molenkamp, F. (1982), "Kinematic Model for Alternating Loading ALTERNAT", LGM Report Co-218598, Delft Geotechnics.
6. Nazemi, A.H. (1998), Modelling of Partially Saturated Soil, UMIST, Ph.D Thesis.
7. Nemat-Nasser, S. (1982), "Fabric and its Influence on Mechanical Behaviour of Granular Material", IUTAM Conf. on Deformation and Failure of Granular Material, Delft, Balkema, pp.37~42.
8. Skempton, A.W. (1960), Pore Pressure and Suction in Soils: Effective Stress in Soils Concrete and Rocks, Butterworth, pp.4~16.
9. Thornton, C. (2000), "Numerical Simulations of Deviatoric Shear Deformation of Granular Media", Geotechnique, 50, pp.43~53.
10. Woodward, P.K. and Molenkamp, F. (1999), "Application of an Advanced Multi-surface Kinematic Constitutive Soil Model", Int. J. Numer. Anal. Meth. Geomech., 23, pp.1995~2043

(received on May 30, 2001)